Revision 1

Word count: 7429 (without tables)

Scandian actinolite from Jordanów, Lower Silesia, Poland: compositional evolution, crystal structure and genetic implications

Adam Pieczka[1*], Marcin Stachowicz[2], Sylwia Zelek-Pogudz[1], Bożena Gołębiowska[1], Mateusz Sęk[1], Krzysztof Nejbert[2], Jakub Kotowski[2], Beata Marciniak-Maliszewska[2], Adam Szuszkiewicz[3], Eligiusz Szełęg[4], Katarzyna M. Stadnicka[5], and Krzysztof Woźniak[6]

[1] AGH University of Science and Technology, Department of Mineralogy, Petrography and Geochemistry, 30-059 Kraków, Mickiewicza 30, Poland, e-mail: pieczka@agh.edu.pl

[2] University of Warsaw, Faculty of Geology, 02-089 Warszawa, Żwirki and Wigury 93, Poland

[3] University of Wrocław, Institute of Geological Sciences, 50-204 Wrocław, pl. M. Borna 9, Poland

[4] University of Silesia, Faculty of Natural Sciences, Institute of Earth Sciences, 41-200 Sosnowiec, Będzińska 60, Poland

[5] Jagiellonian University in Kraków, Faculty of Chemistry, 30-387 Kraków, Gronostajowa 2, Poland

[6] University of Warsaw, Department of Chemistry, 02-093 Warszawa, Pasteura 1, Poland

Abstract

[*] Corresponding author: Adam Pieczka; e-mail: pieczka@agh.edu.pl

This is the peer-reviewed, final accepted version for American Mineralogist, published by the Mineralogical Society of America.
The published version is subject to change. Cite as Authors (Year) Title. American Mineralogist, in press.
DOI: https://doi.org/10.2138/am-2022-8786. http://www.minsocam.org/

Scandian actinolite evolving to scandio-winchite (up to 5.45 wt% Sc_2O_3) has been found in chlorite-dominant xenoliths incorporated into marginal portion of a granitic pegmatite. The pegmatite intruded a blackwall schist zone developed around rodingite-type rocks exposed in a serpentinite quarry at Jordanów Śląski near Sobótka, ~30 km south of Wrocław, Lower Silesia, Poland. The amphiboles form irregular overgrowths around cascandite and represent a complex solid-solution series among actinolite and scandio-winchite end-members, with a trace contribution of 'scandio-magnesio-hornblende'. Structural studies of a scandian actinolite crystal with composition $^{A}(\square_{0.995(2)}K_{0.005(2)})_{\Sigma 1}{}^{B}(Na_{0.24(5)}Ca_{1.73(4)})_{\Sigma 1.98(1)}{}^{C}(Mg_{3.74(7)}Fe^{2+}_{0.90(3)}Mn_{0.04(1)}Sc_{0.26(3)}Al_{0.05(1)})_{\Sigma 4.99(1)}{}^{T}(Si_{7.98(2)}Al_{0.02(2)})_{\Sigma 8.00}O_{22}(OH)_2$ revealed monoclinic $C2/m$ structure with unit-cell parameters a = 9.8517(3), b = 18.0881(6), c = 5.28501(18) Å, β = 104.809(4)°, in which scandium is located solely at the ^{C}M2 site. Scandian amphiboles are uncommon in geological environments, and invite comments on the origin of the observed Sc enrichment in the amphibole structure. Textural appearance of the chlorite-cascandite-amphibole clusters suggests that the formation of the amphiboles is related to the evolution of the country rocks followed by partial alteration of blackwall schist xenoliths by pegmatite-forming melt.

Keywords: scandium, amphibole, scandian actinolite, scandio-winchite, composition, structure refinement, origin.

Introduction

Amphiboles, together with clinopyroxenes, are considered main mineral concentrators of scandium in magmatic deposits responsible for global Sc resources. The concentration of Sc in these minerals only exceptionally reaches 500 ppm (e.g., Tilling et al. 1969; Foord et al. 1993;

Shimazaki et al. 2008; Wang et al. 2020). As a major constituent, scandium has been recognized in compositionally unusual edenite and actinolite with up to 1.7 and 2.9 wt% Sc_2O_3, respectively, from granitic pegmatites and their metagabbro host from the Crystal Mountain fluorite deposit, Ravalli County, Montana, U.S.A. (Foord et al. 1993). On the other hand, scandian analogues of fluor-eckermannite, fluor-nyböite, pargasite and fluor-pargasite, have been synthesized (Raudsepp et al. 1987a, b, 1991; Oberti et al. 1999). Thus, it seems that the incorporation of significant amount of Sc into the amphibole structure can be possible in certain geologic environments.

Amphiboles have the general formula $AB_2C_5T_8O_{22}W_2$ (Hawthorne et al. 2012), where:

A = □, Na, K, Ca, Pb, and Li;

B = Na, Ca, Mn^{2+}, Fe^{2+}, Mg, and Li;

C = Mg, Fe^{2+}, Mn^{2+}, Zn, Co, Ni, Al, Fe^{3+}, Mn^{3+}, Cr^{3+}, V^{3+}, Ti^{4+}, Zr, and Li;

T = Si, Al, Ti^{4+}, and Be;

W = (OH), F, Cl, and O^{2-}.

Scandium is considered a C-group cation that is ordered mainly at the M2 site. However, its site preferences have been studied only in synthetic crystals (Raudsepp et al. 1987a, b, 1991; Oberti et al. 1999), and crystal chemical data from natural Sc-rich amphiboles is lacking.

In this paper we describe a mineral assemblage with cascandite and Sc-enriched amphiboles, including unusually Sc-rich actinolite with up to 5.45 wt% Sc_2O_3, that was found in a wall-rock xenolith incorporated into a marginal portion of a granitic pegmatite at Jordanów Śląski near Sobótka, ~30 km south of Wrocław, Lower Silesia, Poland. Chemical composition of cascandite and scandian actinolite has been studied in details using electron microprobe and the crystal structure of the scandian actinolite has been analyzed by means of single-crystal X-ray diffraction. Based on the obtained results, the site occupancy of Sc in the amphibole structure is

carefully evaluated, and substitution mechanisms controlling the incorporation of Sc into the amphibole structure are discussed. Finally, we discuss the possible mode of origin of the described Sc-rich minerals from Jordanów Śląski in order to add to our understanding of processes leading to crystallization of Sc-rich amphiboles in general, and Sc mineralization in this section of the European Variscides in particular.

Geological setting

Rock samples bearing scandian actinolite were encountered in a serpentinite quarry situated ~1 km west of Jordanów Śląski (formerly Jordansmühl), a village near Sobótka, ~30 km south of Wrocław, Lower Silesia, SW Poland (50°52′16″N 16°50′18″E). The quarry, now practically abandoned, is well known as the first European occurrence of nephrite to be described (Traube 1885a, b). Geologically, it is located near the eastern margin of a ~23 × 11 km serpentinite exposure, the so-called Gogołów-Jordanów Serpentinite Massif (Fig. 1). Together with gabbros, metagabbros and amphibolites that crop out to the northwest, the rocks form the Early Devonian Ślęża Ophiolite located in the Sudetes, the northeastern margin of the Bohemian Massif in the Central European Variscides. The emplacement of the Ślęża Ophiolite has been established at ~400 Ma (Kryza and Pin 2010; Awdankiewicz et al. 2021).

In the Jordanów quarry, the antigorite serpentinites are cut by two roughly NE–SW- trending subvertical to steeply dipping bodies traditionally called leucocratic zones. These have been a subject of several mineralogical and petrological studies. The larger one, ~20–25 m wide, is located in the NE part of the quarry and according to Heflik (1967) represents rodingite-type rocks formed from a gabbroic protolith. Another leucocratic zone, ~5 m wide, is exposed in the western part of the quarry. The research samples come from the thinner leucocratic zone. Here, the exocontact with the surrounding serpentinite is made of discontinuous and tectonically

disrupted blackwall schist, from a few cm to ~1 m thick, containing vermiculite, chlorite, tremolite, and locally also talc (Dubińska and Wiewióra 1988; Dubińska and Szafranek 1990). It also hosts up to ~1.5 × 0.5 m large irregular bodies of nephrite, nephrite schists, and rocks transitional between nephrite and serpentinite as well as between nephrite and blackwall schist. All these nephritic rock types are composed of varying proportions of antigorite, tremolite and chlorite with minor actinolite, diopside, and a number of accessory minerals including grossular-katoite garnet, clinozoisite, prehnite, magnetite, Fe^{3+}-bearing chromite, titanite, zircon, and apatite among others (Gil 2013; Gil et al. 2015, 2020 and references therein). The surrounding serpentinite consists mostly of antigorite with subordinate chrysotile with no relics of primary mafic silicates (Dubińska and Szafranek 1990; Gil et al. 2015, 2020 and references therein).

The leucocratic zone displays a very complex polygenetic mineralogy and intricate structural relationships among various rock types that include rodingites, rodingite-like rocks, partly rodingitized rock of plagiogranitic appearance, and leucogranite (Dubińska 1995). These rocks are tectonized to various extent and interlocking with each other, their mutual structural relationships being complicated and obscured by the poor state of the exposure. In addition, they show effects of low-temperature hydrothermal to supergene alteration manifested by the presence of opal, chalcedony, smectites, and Fe-oxides, among others. The rodingites show very diverse mineralogy, dominated by grossular-rich garnet, zoisite-clinozoisite, epidote, diopside, among others. Various specific subtypes have been distinguished basing on textures and mineralogical composition (Heflik 1967; Majerowicz 1984; Dubińska 1995). In this paper, these rock types will be collectively called metasomatites. Ophiolite-related plagiogranite (Dubińska 1995) or ~340 Ma granitic dike (Kryza 2011; Gil et al. 2020) have been suggested as their possible igneous precursors.

Similarly, various textural types of granitic rocks are present in the leucocratic zone (e.g., Lis and Sylwestrzak 1981; Dubińska and Szafranek 1990; Dubińska 1995; Kryza 2011). Descriptions by various authors differ in details, but fine-grained aplitic, medium-grained granitic and pegmatitic varieties can generally be distinguished. The published descriptions and our own observations show that the assemblage mainly consists of quartz, sodic plagioclase and microcline with minor biotite and muscovite. In the pegmatitic variety, Lis and Sylwestrzak (1981) found mineralization typical of granitic pegmatites with beryl, almandine-spessartine, black tourmaline, columbite-group minerals, gahnite, and probably also fluorite and cassiterite. They proposed that the pegmatitic mineralization can be genetically related to the ~295–305 Ma Strzegom–Sobótka granitic massif, adjacent to the Ślęża Ophiolite on the west. Kryza (2011) dated the medium-grained granite variety at 337 ± 4 Ma, and linked its formation to ~340 Ma felsic magmatism (Oliver et al. 1993; Pietranik et al. 2013) known from the Niemcza Zone, a geological unit that abuts the Ślęża Ophiolite on the south. Although scientific interest in various rocks dates back to the end of 1800s, it is noteworthy that Sc mineralization has not been reported from the Jordanów Śląski quarry until now.

Material and methods

Material

Scandian amphibole of the actinolite type was found in a small fragment of a granitic pegmatite, collected at the end of 1990s by A.P, that is strongly similar to the 'pegmatite with sugary albite' described by Lis and Sylwestrzak (1981). Quartz, sodic plagioclase, K-feldspar and dark green dravite are the main mineral components, whereas pale green to nearly colorless beryl is subordinate. Detailed electron-probe microanalysis, supported in some cases by Raman spectroscopy, revealed the presence of aikinite, allanite-(Ce), bavenite-bohseite, biotite,

cassiterite, clinozoisite, columbite-(Mn), diopside, epidote, fersmite, fluorapatite, galena, polycrase-(Y), monazite-(Ce), muscovite, pyrochlore- and microlite-group minerals, phenakite, rhabdophane-(La), rhabdophane-(Nd), spessartine, titanite, tremolite, zircon, uraninite, xenotime-(Y), and a few Sc-bearing silicates, including scandian actinolite and scandio-winchite. The pegmatite contains irregularly shaped, wavy- and streak-like clusters consisting mostly of chlorite showing jagged contacts with the granitic pegmatite. Unlike the surrounding pegmatite, these chlorite aggregates are porous and show signs of dissolution. In places, they contain parallel, more rarely fan-shaped and radial aggregates of euhedral acicular amphiboles that seem to replace chlorite (Fig. 2). The size of the chlorite and amphibole crystals as well as the overall textural appearance of the chlorite-amphibole clusters strongly resemble chlorite schist from the blackwall bordering the leucocratic zone (cf., Gil 2013; Gil et al. 2015). For instance, scandian actinolite overgrowing cascandite in our samples is similar in shape and size to tremolite replacing chlorite described by Gil et al. (2015) from rocks transitional between nephrite, nephrite schist and chlorite schist. We interpret the chlorite clusters as dismembered and partly assimilated blackwall schist xenoliths. The Sc-rich amphiboles were found exclusively within such xenoliths. Scandian actinolite is spatially associated with cascandite, $CaScSi_3O_8(OH)$. In some cases, the actinolite overgrows fractured and probably also slightly corroded cascandite (Fig. 2a, c, and e), whereas in other places the mutual relationships of the two minerals are not clear (Fig. 1g).

Electron-probe microanalysis (EPMA)

Quantitative chemical analyses were performed at the Inter-Institute Analytical Complex for Minerals and Synthetic Substances at the University of Warsaw, Poland, with a CAMECA SX 100 electron microprobe operating in wavelength-dispersive X-ray spectrometry mode. The following operating conditions were used: accelerating voltage 15 kV; beam current 10 nA; beam

diameter 2 μm; peak and background count times 20 and 10 s, respectively. We employed the following analytical reference materials, emission lines, diffracting crystals, and mean detection limits (in wt.% element): diopside: Mg (*K*α, TAP, 0.02), Si (*K*α, TAP, 0.03), and Ca (*K*α, LPET, 0.02), albite: Na (*K*α, TAP, 0.06), orthoclase: Al (*K*α, LPET, 0.02) and K (*K*α, LPET, 0.02), Sc metallic: Sc (*K*α, LPET, 0.02), rutile: Ti (*K*α, LPET, 0.02), rhodonite: Mn (*K*α, LIF, 0.06), and hematite: Fe (*K*α, LIF, 0.06). Fluorine (*K*α, PC0, 0.13) and Zr (*K*α, LIF, 0.05) were sought but found to be below the detection limits of the microprobe in the scandian actinolite and cascandite; cascandite does not contain potassium either. The raw data were reduced with the PAP routine (Pouchou and Pichoir 1991).

Atomic contents in the empirical amphibole formulae were normalized on the basis of 22 O + 2 (O,OH) ions per formula unit (pfu) using the Excel spreadsheet designed to classify amphiboles (Locock 2014) according to the IMA 2012 recommendations (Hawthorne et al. 2012). For cascandite, the empirical formula was normalized on the oxygen content of $8.5 + x/2$ apfu following the idealized formula proposed by Mellini and Merlino (1982), $^{M1}Ca^{M2}(Sc_{1-x}M^{2+}_{x})^{A}(M^{2+}_{x}\square_{1-x})^{T}Si_3O_{8+x}(OH)_{1-x}$, where $x \cong 0.1–0.2$. The variable x corresponds to the content of M^{2+} cations replacing Sc (and other trivalent cations) at the M2 site. The amount of Fe^{3+} was obtained by matching of Fe^{3+}/Fe_{total} ratio to meet the condition that the content of $^{M2}M^{2+}$ is equal to the content of $^{A}M^{2+}$. The formula is charge-balanced by the adjusting amounts of OH^{-} and O^{2-}.

Single-crystal X-ray diffraction and structure refinement

A single crystal of scandian actinolite, 0.020 × 0.017 × 0.008 mm, was prepared using Quanta 3D 200i (Thermo Fisher Scientific) scanning electron microscope equipped with Ga+ ion gun, Pt precursor gas-injection systems (GIS) and Omniprobe micromanipulator for *in situ* lift-out. Ion beam accelerating voltage of 30 kV and ion currents in the range of 60–1 nA were applied. The

188 sample was transferred *via* a micromanipulator to standard TEM copper half-ring grids. The FIB
189 deposition process (from Pt precursor) was used to attach the manipulator probe to the sample
190 and the foil to the grid. Then the crystal was transferred to a suitable microloop and placed on the
191 goniometer base.

192 Single-crystal X-ray diffraction measurements were made at the Faculty of Chemistry,
193 Jagiellonian University, Kraków, Poland. X-ray diffraction data for a single crystal were
194 collected using XtalLAB Synergy-S (Rigaku - Oxford Diffraction) four-circle diffractometer with
195 a mirror monochromator and a microfocus Mo$K\alpha$ or Cu$K\alpha$ radiation sources. The data were
196 collected at 100.0(2) K using Cu$K\alpha$ radiation (λ = 1.54184 Å) to a maximum θ value of 72.228°.
197 The obtained datasets were processed with CrysAlisPro v171.41.93a software (Rigaku-Oxford
198 Diffraction 2019).

199 The crystal structure of scandian actinolite was solved with dual-space iterative phasing
200 algorithm implemented in ShelXT (Sheldrick 2015a) that located the positions of all cations
201 (except hydrogen) and O anions. Correct element-assignment for cations and anions was based
202 upon compositional data obtained by EPMA and crystal-chemical reasoning, comprising site-
203 scattering, coordination and bond lengths. The model was refined with the least-squares
204 minimization to R_1 = 5.87% using Shelxl (Sheldrick 2015b), with Olex2 (Dolomanov et al. 2009)
205 as the graphical interface. Where more than one element occupies the same position in the
206 asymmetric unit, constraints for equal atom coordinates and equal anisotropic displacement
207 parameters for these groups of atoms at each site were applied. The occupancies of the T2, M1,
208 M2, M3, and M4 sites were refined as Si vs. Al, Mg vs. Fe, Mg vs. Sc, Mg vs. Fe, and Ca vs. Na,
209 respectively, assuming full occupancy of the sites. The T1 site-occupancy was fixed as $Si_{1.00}$, and
210 0.01 K apfu was fixed at the A site. In a recent study of tremolite, Ballirano et al. (2021)
211 presented a successful refinement of the oxygen and silicon structural sites with mixed scattering-

212 factors for ions and atoms. They used high-angle single-crystal X-ray diffraction data $\sin\theta/\lambda \geq$
213 0.91, for which the model converged to R_1 = 1.47%. This improved the fit to X-ray intensities by
214 0.17% compared to standard refinement, where only scattering factors for atoms were used.
215 Considerable correlations in the least-squares refinement were observed with a lower resolution
216 of $\sin\theta/\lambda \geq 0.7$. With the available X-ray data in this study (R_1 = 5.87% and resolution of $\sin\theta/\lambda \geq$
217 0.62), all atoms were refined with scattering factors for atoms.
218

219 **Results**

220 **Composition of cascandite**

221 Cascandite identified in the samples from Jordanów Śląski shows a relatively homogeneous
222 chemical composition (Table 1). In principle, silicon is the only T site occupant. The M2 sites are
223 Sc-dominated with up to 0.93 apfu in a single analytical spot and ~0.75–0.80 apfu in averaged
224 compositions. The charge-balance calculations of the $^{M2}Fe^{3+}$ contents indicate that practically all
225 Fe must occur as ferric iron. In such case, the amounts of M^{2+} cations substituting for Sc at the
226 M2 site approximate the surplus of Na + M^{2+} + M^{3+} cations greater than 2 apfu, which occupies
227 the A site according to the coupled substitution $^{A}M^{2+} + {}^{M2}M^{2+} + O^{2-} \rightarrow {}^{A}\square + {}^{M2}Sc^{3+} + OH^{-}$. This
228 fact is in conflict with common opinion that Sc deficiency in cascandite is compensated mainly
229 by M^{2+} cations including Fe^{2+}. This view probably results from the assumption that all iron in
230 cascandite occurs as Fe^{2+} (Mellini and Merlino 1982). The total amounts of $^{M2}M^{3+}$ cations (Sc +
231 Fe^{3+} + Al) are high and exceed 0.90 apfu. The residual occupancy of the M2 site is filled by M^{2+}
232 cations, mainly Mg, rarely Mn^{2+}, and exclusively Fe^{2+}. The M1 site is occupied by ≤ 0.90 apfu Ca
233 and minor Mn^{2+}, in some cases with traces of Mg. The A site remains largely vacant with minor
234 Ca and traces of Na.

This is the peer-reviewed, final accepted version for American Mineralogist, published by the Mineralogical Society of America.
The published version is subject to change. Cite as Authors (Year) Title. American Mineralogist, in press.
DOI: https://doi.org/10.2138/am-2022-8786. http://www.minsocam.org/

Composition of scandian actinolite

Table 2 presents average compositions of the scandian amphiboles overgrowing cascandite. The vast majority of the studied crystals belong to the calcium amphiboles subgroup of the ^{W}(OH, F, Cl)-dominant amphiboles, with $^{B}(Ca + \Sigma M^{2+})/\Sigma B \geq 0.75$ and $^{B}Ca/\Sigma B \geq {}^{B}\Sigma M^{2+}/\Sigma B$ (Hawthorne et al. 2012). Only in a few analytical spots, the compositions correspond to the sodium-calcium amphiboles subgroup as defined by $0.75 > {}^{B}(Ca + \Sigma M^{2+})/\Sigma B > 0.25$ and $^{B}Ca/\Sigma B \geq {}^{B}\Sigma M^{2+}/\Sigma B$. Increasing content of ^{B}Na is coupled with an increase of $^{C}M^{3+}$ cations, mainly Sc^{3+}. This suggests a simple coupled substitution $^{B}Na^{+} + {}^{C}Sc^{3+} \rightarrow {}^{B}Ca^{2+} + {}^{C}M^{2+}$ as a mechanism responsible for the incorporation of Sc^{3+} in the amphibole structure. As a result, a solid solution between actinolite, $\square Ca_2Mg_{2.5\leq x<4.5}Fe^{2+}_{2.5\geq 1-x>0.5}Si_8O_{22}(OH)_2$, and scandio-winchite species, $\square(NaCa)(Mg_4Sc)Si_8O_{22}(OH)_2$, is formed (Fig. 3). The covariation (in apfu) $^{C}(Al+Fe^{3+}+Sc+2Ti)$ vs. ^{B}Na is described by the equation: $y = 0.968 \cdot x + 0.126$ ($R^2 = 0.815$). The y-intercept of the formula, equal to 0.126 Sc apfu, indicates that another Sc end-member must also be present. This end-member can be related to coupled replacements at the M1-M3 and T sites according to the equation $^{M1\text{-}M3}Sc^{3+} + {}^{T}Al^{3+} \rightarrow {}^{M1\text{-}M3}M^{2+} + {}^{T}Si^{4+}$, leading to a hypothetical 'scandio-magnesio-hornblende', $\square Ca_2(Mg_4Sc)(Si_7Al)O_{22}(OH)_2$. In fact, in the Excel spreadsheet designed for the formula calculation and species identification of amphiboles (Locock 2014) such compositions are identified as magnesio-hornblende. However, the hypothetical species should be referred to as 'scandio-magnesio-hornblende' because ^{C}Sc predominates over ^{C}Al.

On the basis of textural relations between the cascandite core and scandian amphibole overgrowths in the aggregates (Fig. 2), we propose the following sequence of crystallization with decreasing Sc activity: cascandite → scandio-winchite → 'scandio-magnesio-hornblende' → scandian actinolite. Scandio-winchite has been recently approved by the IMA CNMNC (Pieczka et al. 2022). 'Scandio-magnesio-hornblende' may represent a new species, but additional research

is required. Potentially, this species would be a Sc-bearing analogue of magnesio-hornblende, $\square Ca_2(Mg_4Al)(Si_7Al)O_{22}(OH)_2$, in which Al is a trivalent cation ordered at the M2 sites. Therefore, this hypothetical species should have the end-member composition $\square Ca_2(Mg_4Sc)(Si_7Al)O_{22}(OH)_2$, with one Al cation pfu placed at the T site. All the compositions tentatively identified as 'scandio-magnesio-hornblende' (Table 2), described in the idealized form in accordance with the dominant-constituent rule (Hatert and Burke 2008), give a charge-unbalanced formula $\square Ca_2(Mg_4Sc)Si_8O_{22}(OH)_2$ with T sites fully occupied by Si. Consequently, crystals with such compositions cannot be considered as true 'scandio-magnesio-hornblende'. The 'scandio-magnesio-hornblende' end-member makes up only a small fraction of these compositions and can be calculated as being equal to $^{T}Al^{3+}$. In fact, such compositions of Sc-bearing actinolite must be treated as a complex solid-solution series of three end-members:

1. scandio-winchite, $\square(NaCa)(Mg_4Sc)Si_8O_{22}(OH)_2$,
2. 'scandio-magnesio-hornblende', $\square Ca_2(Mg_4Sc)(Si_7Al)O_{22}(OH)_2$,
3. actinolite, $\square Ca_2Mg_{2.5\leq x<4.5}Fe^{2+}_{2.5\geq 1-x>0.5}Si_8O_{22}(OH)_2$.

Quantitatively, proportions of these end-members can be defined by the following compositional variables:

- scandio-winchite by $^{B}Na + 2\cdot{}^{B}\square$,
- 'scandio-magnesio-hornblende' by $^{T}M^{3+}$,
- actinolite by $(^{B}M^{2+} - 3\cdot{}^{B}\square - {}^{B}Na - 2\cdot {}^{T}M^{3+})/2$,

where $^{B}\square$ is a small deficiency of B-cations in the amphibole formula. It can be explained by a limited substitution $^{B}\square + {}^{B}Ca \rightarrow 2\,{}^{B}Na$. In the case of some of the compositions obtained for the scandian amphiboles from Jordanów Śląski that were tentatively identified as 'scandio-magnesio-hornblende', the three end-members are present with the contents (in mol%) of scandio-winchite:

44.9, 51.1, 52.8, and 56.2; 'scandio-magnesio-hornblende': 7.6, 1.3, 4.6, and 5.8; and actinolite: 47.5, 47.6, 42.6, and 38.0, respectively, in the samples J6, J10, J5 and J4. Thus, the compositions represent scandio-winchite or actinolite species with only very low, but non-negligible, proportion of 'scandio-magnesio-hornblende'.

Crystal-structure refinement

The crystal of scandian actinolite extracted for structure refinement has the EPMA-derived composition (Table 2, last column) $^{A}(\square_{0.995(2)}K_{0.005(2)})_{\Sigma 1}{}^{B}(Na_{0.24(5)}Ca_{1.73(4)})_{\Sigma 1.98(1)}{}^{C}(Mg_{3.74(7)}Fe^{2+}{}_{0.90(3)}Mn_{0.04(1)}Sc_{0.26(3)}Al_{0.05(1)})_{\Sigma 4.99(1)}{}^{T}(Si_{7.98(2)}Al_{0.02(2)})_{\Sigma 8.00}O_{22}(OH)_2$ (estimated standard deviations in parentheses). Its structure was solved and refined to an R_1 value of 5.87%. Data collection and structure refinement details are presented in Table 3. Atom positions, equivalent isotropic displacement parameters and selected interatomic distances are in the attached CIF file; Table 4 presents assigned site-populations, and Table 5 provides bond-valence analysis of the scandian actinolite.

The T sites are generally filled with Si as indicated by the EPMA results and the refined T1 and T2 site-scatterings as well as mean bond-lengths of 14.00 and 13.98 e^-, and 1.622 and 1.636 Å, respectively. As for the two sites, T1 was accepted as occupied only by Si, and T2 site contains most likely a small amount of Al substituting for Si, which, considering standard deviation (σ) of the EPMA-derived ^{T2}Al content and T2 site-scattering, can range from 0 to 0.07 apfu. The M1–M3 and M4 sites are completely occupied by Mg, Fe^{2+}, Mn^{2+}, Sc and Al, and by Ca and Na, respectively. The normalized EPMA-derived atomic contents indicate total electron-density of 75.5 e^- at the five M1–M3 sites, and 37.3 e^- at the two M4 site. The structure refinement indicates respectively total site-scattering at the M1–M3 sites of 73.30(75) e^- and 36.2(3) e^- at the M4 site. The differences between the results from EPMA and SREF measurements do not exceed 3σ. The optimized actinolite formula

This is the peer-reviewed, final accepted version for American Mineralogist, published by the Mineralogical Society of America.
The published version is subject to change. Cite as Authors (Year) Title. American Mineralogist, in press.
DOI: https://doi.org/10.2138/am-2022-8786. http://www.minsocam.org/

306 $^{A}(\square_{0.995}K_{0.005})_{\Sigma1}{}^{B}(Na_{0.29}Ca_{1.71})_{\Sigma2}{}^{C}(Mg_{3.81}Fe^{2+}{}_{0.84}Mn_{0.04}Sc_{0.25}Al_{0.06})_{\Sigma5}{}^{T}(Si_{7.98}Al_{0.02})_{\Sigma8}O_{22}(OH)_2$ was
307 obtained by adding not more than 1.75 of the respective standard deviations to SREF-derived
308 values (Table 4). The refined M1 to M3 populations correspond to the total site-scatterings of
309 29.18(28), 29.56(29), and 14.56(18) e^-, respectively, which increased by the respective σ values
310 multiplied by 1.75 give the scatterings of 29.67(49), 30.06(51), and 14.88(32) e^-. They allow
311 optimization of the M1, M2 and M3 site-populations at:
312 M1: $(Mg_{1.59}Fe^{2+}{}_{0.39}Mn_{0.02})_{\Sigma2}$
313 M2: $(Mg_{1.48}Fe^{2+}{}_{0.25}Mn_{0.02}Sc_{0.25})_{\Sigma2}$
314 M3: $(Mg_{0.74}Fe^{2+}{}_{0.20}Al_{0.06})_{\Sigma1}$
315 for which the <(M1-M3)–O> mean bond-lengths (m.b.l.) of 2.093, 2.092, and 2.081 Å,
316 calculated based on the effective radii by Shannon (1976), give similar differences (0.009–0.013
317 Å) with respect to the refined values.
318 Table 5 presents bond-valence analysis of the occupancy model with Sc located only at the
319 M2 site. It corroborates the assigned M4, T1 and T2 site-occupancies, and the presence of Sc at
320 the M2 site although bond-valence sums (BVS) for the all M1–M3 sites are slightly increased
321 probably because somewhat shortened (M1 to M3)–O bonds. Other locations of M^{3+} cations than
322 M2 were checked. Aluminum at the M1 or M2 site broadens the range of the observed
323 differences between the calculated and refined m.b.l. to 0.004–0.020 Å, indicating that the M3
324 site is the most likely location of the constituent. The placement of Sc on the M3 site similarly
325 increases the differences, but the placement on the M1 site leads to bond lengths differences in
326 the range 0.009–0.012 Å, comparable to that if Sc is placed at M2. Bond-valence analysis for this
327 case indicates ~2.23, 2.14 and 2.15 v.u. for the M1 to M3 sites, which could be consistent with
328 the M1 site of the Sc. However, based on the IMA-recommended distribution of M^{3+} cations in
329 Mg-rich calcium amphiboles with $W = (OH, F, Cl)_2$ that assigns all M^{3+} cations to the M2 site

except where some Al–Mg disorder takes place over M2 and M3 (Hawthorne et al. 2012), we accepted the above presented M1-to-M3 site-occupancies with all Sc located at the M2 as the most adequate.

The occupancy of the 8-fold-coordinated M4 site was refined at 0.788(16)Ca + 0.212(16)Na for which the corresponding site-scattering is 18.09(14) e^-. It agrees well with the M4-site electron density of 18.69 e^- calculated on the basis of the optimized formula; furthermore, the refined <B–O> m.b.l. of 2.511Å agrees with the value of 2.502 Å calculated on the basis of the optimized formula. The A site remains generally vacant in the structure of scandian actinolite; it contains trace amounts of K^+ [0.005(2) apfu] with <K–O> m.b.l. of 2.963 Å, corresponding to the ^{X}K–O bond of 2.95 Å calculated on the basis of Shannon's (1976) radii.

Genetic implications

The samples of the Jordanów Śląski pegmatite are small and lack contacts with other rock types present in the leucocratic zone. Currently, the state of the exposure in the inactive quarry is poor, and the pegmatite cannot be observed *in situ*. Therefore, it is not possible to place our samples in a broader geologic context. However, the presence of blackwall schist xenoliths suggests that the samples represent a portion of the pegmatite that was in contact with the blackwall rocks and possibly also the rodingite-like metasomatites that constitute most of the leucocratic zone. Brecciation of the metasomatites (Dubińska 1995) facilitated introduction of the wallrock xenoliths during the pegmatite's emplacement. Partial assimilation of the xenoliths resulted in the local enrichment in Ca, Mg and Fe of the melt. This inference is supported by locally abundant Ca-Mg-Fe accessory phases, such as epidote, allanite, clinozoisite, titanite, and diopside.

The occurrence of cascandite – scandian actinolite intergrowths in the pegmatite samples is restricted to the xenoliths. All the observations made so far suggest that uncontaminated

354 pegmatite-forming melt was rather poor in Sc. First of all, assuming that the samples at our
355 disposal are representative to the Jordanów Śląski pegmatite, the pegmatite does not contain
356 significant Sc mineralization in xenoliths-free portions. Such mineralization, however, would be
357 expected as in the absence of abundant ferromagnesian minerals, Sc behaves as an incompatible
358 element and concentrates in residual melts and related orthomagmatic fluids, leading to the
359 crystallization of accessory Sc phases (e.g. Novák and Čech 1995; Novák and Černý 1998;
360 Grammaccioli et al. 2000; Pezzotta et al. 2005; Hreus et al. 2021). This incompatibility of Sc in
361 felsic melts is a result of its high affinity to form strong fluoride complexes (Gramaccioli et al.
362 2000; Pezzotta et al. 2005; Shchekina and Gramenitskiy 2008). Therefore, it might be assumed
363 that if the Jordanów Śląski pegmatite crystallized from a residual melt that became enriched in Sc
364 due to advanced fractionation of a larger batch of magma, it would contain also noticeable F
365 mineralization. However, unlike the pegmatites of Baveno, Italy, where Sc mineralization is
366 commonly associated with abundant F-bearing phases (e.g., Gramaccioli et al. 2000; Pezzotta et
367 al. 2005), the Jordanów Śląski pegmatite lacks F-bearing minerals except for very rare
368 fluorapatite. Traces of fluorine were also noted in titanite and accessory dravite. The presence of
369 fluorite, tentatively identified previously by X-ray diffraction in a polymineral sample by Lis and
370 Sylwestrzak (1981), has not been confirmed in any of over 20 pegmatitic specimens studied by us
371 by electron microprobe. Also no signs of the activity of F-enriched hydrothermal fluid have been
372 observed in the wallrock and the wallrock xenoliths.

373 Interestingly, it was proposed that the most Sc-enriched amphiboles reported so far, i.e.
374 edenite and actinolite (up to 1.7 and 2.9 wt% Sc_2O_3, respectively) from the Crystal Mountain,
375 Ravalli County, Montana, USA, formed due to the assimilation of Sc-rich metagabbro by F-rich
376 pegmatite-forming melts (Foord et al. 1993). However, this scenario is very unlikely in the case
377 of the scandian actinolite from Jordanów Śląski for the reasons mentioned above. Low-degree

partial melting of the mafic-ultramafic rocks, wherein Sc is scavenged from the source rocks by a pegmatite-forming anatectic melt, has been proposed as a mechanism responsible for Sc mineralization in the anatectic pegmatites of Tørdal and Evje-Iveland, Norway (Bergstøl and Juve 1988; Williams-Jones and Vasyukova 2018; Steffennsen et al. 2020). Recent experimental works, however, indicate that magmatic differentiation of the anatectic melt obtained by partial melting of amphibolites was indispensible at least for the formation of the Evje-Iveland pegmatites (Gion et al. 2021). Regardless of whether direct anatexis alone or anatexis coupled by magmatic differentiation is taken into consideration, such model is not applicable to the Jordanów Śląski pegmatite. In contrast to the Tørdal and Evje-Iveland pegmatites, our pegmatite is emplaced in the serpentinites that record zeolite- to greenschist-facies conditions (Majerowicz 1984; Dubińska et al. 2004 and references therein) and cannot be regarded as a potential source for anatectic pegmatite-forming melt. Although we cannot rule out the possibility that the melt originated in more distant tectono-metamorphic domains of the Sudetes, the present state of knowledge does not support the anatectic model for the origin of the Jordanów Śląski pegmatite. Also the current regional geotectonic models of the Ślęża Ophiolite and its surroundings do not account for the presence of a batch of anatectic magma hidden in depth (e.g. Wojtulek et al. 2021 and references therein).

Summing up, currently available textural and mineralogical observations indicate that the formation of the studied cascandite – scandian actinolite intergrowths is related to the geologic evolution of the country rocks rather than to the evolution of the pegmatite. It is also noteworthy that if this hypothesis is correct, assimilation of the blackwall rock xenoliths could have also introduced some Sc into the pegmatite-forming melt. However, such contamination would rather be limited due to the small size of the pegmatite that can be estimated from earlier descriptions (Lis and Sylwestrzak 1981) and our own observations on the order of several decimeters. Such

small pegmatitic bodies are believed to cool rapidly in contact with much cooler country rocks, what would hamper the assimilation process. Consequently, it is reasonable to expect that, apart from xenocrysts and xenolith-related mineral assemblages, potential Sc mineralization in the Jordanów Śląski pegmatite would be volumetrically insignificant.

The content of Sc in cascandite crystals is similar in all the investigated samples and decreases from core to rim (Fig. 2b, d, e). This indicates that Sc was incorporated as a compatible element during mineral growth and became progressively diluted, mainly by Fe^{2+} and Mg. While cascandite is fractured and possibly also slightly corroded, the overgrowing actinolite is euhedral and does not show dissolution textures (Fig. 2a-c). It seems, therefore, that the two minerals formed at separate stages of crystallization involving a destabilization of the cascandite. It is possible that dissolution of cascandite supplied enough Sc to enrich some of the newly formed amphibole up to the compositions of scandian actinolite. It seems also that the actinolite formed at the expense of chlorite. The only amphibole-bearing rock types in close proximity of the pegmatite are nephrite and rocks transitional between nephrite and chlorite schist. Although the nephritic rock is composed predominantly of tremolite, a later generation of actinolitic amphibole also is present (Gil et al. 2015). Besides, the amphibole crystals are similar in shape and size to tremolite replacing chlorite and forming nephrite-like nests in the chlorite schist, as described by Gil et al. (2015). Therefore, the cascandite – scandian actinolite aggregates may well have formed in a similar manner to the amphiboles of the adjacent nephrite-type rocks.

Unfortunately, there is no currently available information on the Sc contents in the rocks from the immediate vicinity of the pegmatite, such as serpentinite, rodingite-like metasomatites, nephrite, and blackwall chlorite schists. To our best knowledge, Sc-bearing minerals have not been observed in the rock suite of the Ślęża Ophiolite. This fact does not preclude the possibility that such mineralization may be present either as dispersed rare accessories or in local-scale

426 concentrations. It should be stressed that the presence of Sc in the Ca minerals can pass unnoticed
427 in routine research because the Sc*K*α line coincides with the Ca*K*β line in the energy-dispersive
428 spectrum. Similarly, the presence of rare minuscule small-sized Sc-minerals can be easily
429 overlooked during routine petrographic studies. The only published whole-rock geochemical
430 analyses of the rodingite-like metasomatites and blackwall schists from the Nasławice quarry,
431 ~1.5 km NW from the Jordanów Śląski quarry, indicate low contents of 3–5 ppm Sc (Dubińska et
432 al. 2004). Other rock types in the Ślęża Ophiolite show variable Sc contents: ~5.1–12 ppm in
433 serpentinites with various proportions of ultramafic relics, 2.79–57.57 ppm in gabbroic rocks, and
434 39.4–46.56 ppm in metabasalts and metadolerites (Lebda 1995; Abdel Wahed 1999; Floyd et al.
435 2002; Dubińska et al. 2004; Wojtulek et al. 2021). It seems that the Sc concentrations in these
436 rocks positively correlate with the amount of clinopyroxene, with the highest values found in the
437 varieties identified as 'diallagite' (Wojtulek et al. 2021) and pyroxenite/gabbro (Abdel Wahed
438 1999; Floyd et al. 2002). This is in agreement with numerous observations indicating
439 clinopyroxene as a major Sc carrier in many igneous complexes worldwide (e.g. Williams-Jones
440 and Vasyukova 2018; Wang et al. 2020). Therefore, it is very likely that magmatic clinopyroxene
441 was the primary magmatic collector of Sc in the Ślęża Ophiolite rock suite and its alteration
442 during regional metamorphism led to the remobilization of Sc. Redistribution of Sc and its local
443 concentration within the ophiolitic rocks may have occurred at that stage. A different source of
444 Sc, external in relation to the ophiolitic rocks, cannot be excluded but presently there are no
445 indications of such process.

446 The origin of cascandite – scandian actinolite intergrowths in the blackwall xenolith present in
447 the pegmatite is apparently related to the amphibole crystallization event responsible also for the
448 origin of the nephritic rocks in the blackwall. A recent model of the Jordanów Śląski nephrite
449 formation (Gil et al. 2015, 2020) points to several stages of crystallization and at least two

450 metasomatic events. The earlier metasomatic event involved fluid-mediated rodingitization of an
451 intrusive precursor and replacement of the adjoining serpentinites and was followed by
452 crystallization of the first generation of amphibole (main nephritization stage). The later one
453 modified the mineral composition of nephrites and could have been involved in the formation of
454 the second generation of amphiboles. On the basis of the U-Pb zircon dating (Kryza 2011), the
455 emplacement age of the partially rodingitized granitic dyke is regarded to be contemporaneous
456 with the ca. 340 Ma felsic magmatism in the Niemcza Zone, the geological unit that adjoins the
457 Ślęża Ophiolite from the south. According to Gil et al. (2020), this correlation is supported by
458 similar initial $^{87}Sr/^{86}Sr$ values of the least evolved Jordanów Śląski nephrites and the Niemcza
459 granites. Also on the basis of the Sr isotopes studies, the later metasomatic event is tentatively
460 correlated by Gil et al. (2020) with the influence of the younger ~305 Ma granites of the
461 Strzegom-Sobótka pluton that bounds the Ślęża Ophiolite from the west.

462 Whereas nephrite is predominantly constituted of tremolite, with actinolite present mostly as a
463 second generation of amphibole (Gil et al. 2015), it is tempting to correlate the crystallization of
464 scandian actinolite with the later metasomatic event. However, as the complex and multistage
465 evolution of the rocks of the leucocratic zone at Jordanów Śląski is still a matter of debate,
466 defining the exact relation of the crystallization of cascandite – scandian actinolite intergrowths
467 to a specific stage in this evolution is premature.

468

469 **Acknowledgements**

470 The authors thank Robert F. Martin and George E. Harlow for their very helpful comments and
471 suggestions, which greatly improved the manuscript. We appreciate also careful editorial
472 handling of Fabrizio Nestola. This study was supported by the National Science Centre (Poland)
473 grant 2019/33/B/ST10/00120 to AP.

References

Abdel Wahed, M. (1999) The Ślęża ophiolite (SW Poland): petrological and structural evolution. 302 p. Ph.D. thesis, University of Wrocław.

Awdankiewicz, M., Kryza, R., Turniak, K., Ovtcharova, M., and Schaltegger, U. (2021) The Central Sudetic Ophiolite (European Variscan Belt): Precise U–Pb zircon dating and geotectonic implications. Geological Magazine, 158, 555–566.

Ballirano, P., Celata, B., Pacella, A., and Bosi, F. (2021) Recommended X-ray single-crystal structure refinement and Rietveld refinement procedure for tremolite. Acta Crystallographica, B77, 537–549.

Bergstøl, S., and Juve, G. (1988) Scandian ixiolite, pyrochlore and bazzite in granite pegmatite in Tordal, Telemark, Norway. A contribution to the mineralogy and geochemistry of scandium and tin. Mineralogy and Petrology, 38, 229–243.

Dolomanov, O.V., Bourhis, L.J., Gildea, R.J., Howard, J.A.K., and Puschmann, H. (2009) OLEX2: a complete structure solution, refinement and analysis program. Journal of Applied Crystallography, 42, 339–341.

Dubińska, E. (1995) Rodingites of the eastern part of the Jordanów - Gogołów serpentinite massif, Lower Silesia, Poland. The Canadian Mineralogist, 33, 585–608.

Dubińska, E., and Szafranek, D. (1990) On the origin of layer silicates from Jordanów (Lower Silesia, Poland). Archiwum Mineralogiczne, 46, 19–36.

Dubińska, E., and Wiewióra, A. (1988) Layer silicates in the contact zone between granite and serpentinite, Jordanów, Lower Silesia, Poland. Clay Minerals, 23, 459–470.

Dubińska, E., Bylina, P., Kozłowski, A., Dörr, W., Nejbert, K., Schastok, J., and Kulicki, C. (2004) U–Pb dating of serpentinization: hydrothermal zircon from a metasomatic rodingite shell (Sudetic ophiolite, SW Poland). Chemical Geology, 203, 183– 203.

Floyd, P.A., Kryza, R., Crowley, Q.G., Winchester, J.A., and Abdel Wahed, M. (2002) Ślęża ophiolite: geochemical features and relationship to Lower Palaeozoic rift magmatism in the Bohemian Massif. In: J.A. Winchester, T.C. Pharaoh, J. Verniers, Eds., Palaeozoic Amalgamation of Central Europe, p. 197–215. Geological Society of London, Special Publications 201.

Foord, E.E., Birmingham, S.D., Demartin, F., Pilati, T., Gramaccioli, C.M., and Lichte, F.E. (1993) Thortveitite and associated Sc-bearing minerals from Ravalli County, Montana. The Canadian Mineralogist, 31, 337–346.

Gagné O.C., and Hawthorne F.C. (2015) Comprehensive derivation of bond-valence parameters for ion pairs involving oxygen. Acta Crystallographica, B71, 562–578.

Gil, G. (2013) Petrographic and microprobe study of nephrites from Lower Silesia (SW Poland). Geological Quarterly, 57, 395–404.

Gil, G., Barnes, J.D., Boschi, C., Gunia, P., Szakmány, G., Bendõ, Z., Raczynski, P., and Péterdi, B. (2015) Origin of serpentinite-related nephrite from Jordanów and adjacent areas (SW Poland) and its comparison with selected nephrite occurrences. Geological Quarterly, 59, 457–472.

Gil, G., Bagiński, B., Gunia, P., Madej, S., Sachanbiński, M., Jokubauskas, P., and Belka, Z., (2020) Comparative Fe and Sr isotope study of nephrite deposits hosted in dolomitic marbles and serpentinites from the Sudetes, SW Poland: implications for Fe-As-Au-bearing skarn formation and post-obduction evolution of the oceanic lithosphere. Ore Geology Reviews, 118, 103335.

520 Gion, A.M., Piccoli, P.M., Fei, Y., Candela, P.A., and Ash, R.D. (2021) Experimental constraints
521 on the formation of pegmatite-forming melts by anatexis of amphibolite: A case study from
522 Evje-Iveland, Norway. Lithos, 398, 106342.
523 Gramaccioli, C.M., Diella, V., and Demartin, F. (2000) The formation of scandium minerals as
524 an example of the role of complexes in the geochemistry of rare earths and HFS elements.
525 European Journal of Mineralogy, 12, 795–808.
526 Hatert, F., and Burke, E.A.J. (2008) The IMA-CNMNC dominant-constituent rule revisited and
527 extended. The Canadian Mineralogist, 46, 717–728.
528 Hawthorne, F.C., Oberti, R., Harlow, G.E., Maresch, W.V., Martin, R.F., Schumacher, J.C., and
529 Welch, M.D. (2012) Nomenclature of the amphibole supergroup. American Mineralogist, 97,
530 2031–2048.
531 Heflik, W. (1967) Studium mineralogiczno-petrograficzne leukokratycznej strefy przeobrażonej
532 okolic Jordanowa Śląskiego (Dolny Śląsk). Prace Mineralogiczne PAN, 10, 122 p.
533 Wydawnictwa Geologiczne (in Polish).
534 Hreus, S., Výravský, J., Cempírek, J., Breiter, K., Vašinová Galiová, M., Krátký, O., Šešulka, V.,
535 and Škoda, R. (2021) Scandium distribution in the world-class Li-Sn-W Cínovec greisen-type
536 deposit: result of a complex magmatic to hydrothermal evolution, implications for scandium
537 valorization. Ore Geology Reviews, 139, 104433.
538 Kryza, R. (2011) Early Carboniferous (~337 Ma) granite intrusion in Devonian (~400 Ma)
539 ophiolite of the Central-European Variscides. Geological Quarterly, 55, 213–222.
540 Kryza, R., and Pin, (2010) The Central-Sudetic ophiolites (SW Poland): Petrogenetic issues,
541 geochronology and palaeotectonic implications. Gondwana Research, 17, 292–305.

Lebda, E.M. (1995) Petrology and mineral chemistry of serpentinite rocks of the Gogołów-Jordanów Massif, SW Poland, 189 p. Ph.D. thesis, Archive of the University of Wrocław, Poland.

Lis, J., and Sylwestrzak, H. (1981) Nowy zespól mineralny w leukokratycznej strefie Jordanowa k. Sobótki jego znaczenie genetyczne. Przegląd Geologiczny, 29, 67–71 (in Polish).

Locock, A.J. (2014) An Excel spreadsheet to classify chemical analyses of amphiboles following the IMA 2012 recommendations. Computers & Geosiences, 62, 1–11.

Majerowicz, A. (1984) Petrography and genesis of rodingites in serpentinites of the Ślęża ophiolitic group (in Polish with English summary). Geologia Sudetica, 18, 109–132.

Mellini, M., and Merlino, S. (1982) The crystal structure of cascandite, $CaScSi_3O_8(OH)$. American Mineralogist, 67, 604–609.

Mellini, M., Merlino, S., and Orlandi, P. (1982) Cascandite and jervisite, two new scandium silicates from Baveno, Italy. American Mineralogist, 67, 599–603.

Novák, M., and Čech, F. (1995) Scandian columbite and niobian rutile from pegmatites penetrating the Třebíč durbachite massif, western Moravia, Czech Republic. Acta Musei Moraviae, Scientiae Naturales, 80, 3–8.

Novák, M., and Černý, P. (1998) Scandium in columbite-group minerals from LCT pegmatites in the Moldanubicum, Czech Republic. Krystalinikum, 24, 73–89.

Oberti, R., Hawthorne, F.C., Cámara, F., and Raudsepp, M. (1999) Unusual M^{3+} cations in synthetic amphiboles with nominal fluoro-eckermannite composition: Deviations from stoichiometry and structural effects of the cummingtonite component. American Mineralogist, 84, 102–111.

564 Oliver, G.J.H., Corfu, F., and Krogh, T.E. (1993) U–Pb ages from SW Poland: evidence for a
565 Caledonian suture zone between Baltica and Gondwana. Journal of the Geological Society,
566 150, 355–369.
567 Pezzotta, F., Diella, V., and Guastoni, A. (2005) Scandium silicates from the Baveno and Cuasso
568 al Monte NYF-granites, Southern Alps (Italy): Mineralogy and genetic inferences. American
569 Mineralogist, 90, 1442–1452.
570 Pieczka, A., Stachowicz, M., Zelek-Pogudz, S., Gołębiowska, B., Nejbert, K., Kotowski, J.,
571 Marciniak-Maliszewska, B., Szuszkiewicz, A., Szełęg, E., Stadnicka, K.M. and Woźniak, K.
572 (2022) Scandio-winchite, IMA 2022-009. CNMNC Newsletter 67; Mineralogical Magazine,
573 86, https://doi.org/10.1180/mgm.2022.56
574 Pietranik, A., Storey, C., and Kierczak, J. (2013) The Niemcza diorites and monzodiorites
575 (Sudetes, SW Poland): a record of changing geotectonic setting at ca. 340 Ma. Geological
576 Quarterly, 57, 325–334.
577 Pouchou, J.L., and Pichoir, F. (1991) Quantitative analysis of homogeneous or stratified
578 microvolumes applying the model “PAP”. In K.F.J. Heinrich, and D.E. Newbury, Eds.,
579 Electron Probe Quantitation. Springer, Boston, MA.
580 Raudsepp, M., Turnock, A., Hawthorne, F.C., Sheriff, B., and Hartman J.S. (1987a)
581 Characterization of synthetic pargasitic amphiboles $NaCa_2Mg_4M^{3+}Si_6Al_2O_{22}(OH,F)_2$; M^{3+} =
582 Al, Cr, Ga, Sc, In) by infrared spectroscopy, Rietveld structure refinement, and ^{27}Al, ^{29}Si, and
583 ^{19}F MAS-NMR spectroscopy. American Mineralogist, 72, 580–593.
584 Raudsepp, M., Turnock, A., and Hawthorne, F.C. (1987b) Characterization of cation ordering in
585 synthetic scandium-fluor-eckermannite, indium-fluor-eckermannite, and scandium-fluor-
586 nyböite by Rietveld structure refinement. American Mineralogist, 72, 959–964.

587 Raudsepp, M., Turnock, A., and Hawthorne, F.C. (1991) Amphiboles at low pressure: what
588 grows and what doesn't. European Journal of Mineralogy, 3, 983–1004.
589 Rigaku Oxford Diffraction (2019) CrysAlisPro Software system, version 1.171.40.67a, Rigaku
590 Corporation, Wroclaw, Poland.
591 Shannon, R.D. (1976) Revised effective ionic radii and systematic studies of interatomic
592 distances in halides and chalcogenides. Acta Crystallographica, A32, 751–767.
593 Shchekina, T.I., and Gramenitskii, E.N. (2008) Geochemistry of Sc in the magmatic process:
594 Experimental evidence. Geochemistry International, 46, 351–366.
595 Sheldrick, G.M. (2015a) Crystal structure refinement with SHELXL. Acta Crystallographica,
596 C71, 3–8.
597 Sheldrick, G.M. (2015b) SHELXT – Integrated space-group and crystal-structure determination.
598 Acta Crystallographica, A71, 3–8.
599 Shimazaki, H., Yang, Z., Miyawaki, R., and Shigeoka, M. (2008) Scandium-bearing minerals in
600 the Bayan Obo Nb-REE-Fe deposit, Inner Mongolia, China. Resource Geology, 58, 80–86.
601 Steffenssen, G., Muller, A., Munnik, F., Friis, H., Erambert, M., Kristoffersen, M., and Rosing-
602 Schow, N. (2020) Unusual scandium enrichments of the Tørdal pegmatites, south Norway.
603 Part I: Garnet as Sc exploration pathfinder. Ore Geology Reviews, 126, 103729.
604 Tilling, R.I., Greenland, L.P., and Gottfried, D. (1969) Distribution of scandium between
605 coexisting biotite and hornblende in igneous rocks. Geological Society of America Bulletin,
606 80, 651–668.
607 Traube, H. (1885a) Über den Nephrit von Jordansmuhl in Schlesien. Neues Jahrbuch für
608 Mineralogie, Geologie und Paleontologie, Beilage-Band, 3, 412–427.
609 Traube, H. (1885b) Über den Nephrit von Jordansmühl in Schlesien. Neues Jahrbuch für
610 Mineralogie, Geologie und Paleontologie, Beilage-Band, 2, 91–94.

611 Wang, Z., Yan Hei Li, M., Ray Liu, Z.R., and Zhou, M.F. (2020) Scandium: ore deposits, the
612 pivotal role of magmatic enrichment and future exploration. Ore Geology Reviews, 128,
613 103906.
614 Warr, L.N. (2021) IMA–CNMNC approved mineral symbols. Mineralogical Magazine, 85, 291–
615 320.
616 Williams-Jones, A.E., and Vasyukova, O.V. (2018) The economic geology of scandium, the runt
617 of the rare earth element litter. Economic Geology, 113, 973–988.
618 Wojtulek, P.M., Schulz, B., Klemd, R., Gil, G., Dajek, M., and Delura, K. (2021) The Central-
619 Sudetic ophiolites – remnants of the SSZ-type Devonian oceanic lithosphere in the European
620 part of the Variscan Orogen. Gondwana Research, 105, 343–365.
621

Figure captions:

Figure 1. Geological map of the Gogołów - Jordanów Śląski serpentinite massif and the associated geological units.

Figure 2. Back-scattered electron images and Sc X-ray maps of the cascandite – scandian actinolite aggregates in the Jordanów Śląski pegmatite: (**a**–**d**) sample J5, (**e**–**f**) sample J6, (**g**) sample J10. Abbreviations of mineral names: Act – actinolite, Cas – cascandite, Clc – clinochlore, Fsp – feldspar, Ttn – titanite (Warr 2021).

Figure 3. A covariation $^{C}(Al + Sc + 2Ti)$ vs. ^{B}Na. Symbols: grey diamonds – scandian actinolite, pink diamonds – scandio-winchite, green diamonds – solid-solution members corresponding to ‘ scandio-magnesio-hornblende’.

Table 1. Compositions of cascandite.

Sample	J6	J10	J5
wt%	n=17[a]	n=8	n=17
SiO_2	56.15(55)	56.52(55)	56.77(61)
TiO_2	0.05(2)	0.04(1)	0.04(1)
Al_2O_3	0.28(16)	0.15(10)	0.22(22)
Sc_2O_3	16.51(135)	16.37(72)	17.32(148)
Fe_2O_3	3.61(87)	3.80(64)	2.88(91)
MnO	1.76(48)	2.00(27)	1.67(50)
MgO	1.10(23)	0.85(19)	0.88(37)
CaO	16.96(35)	17.31(19)	17.15(83)
Na_2O	0.05(5)	0.05(3)	0.03(4)
$H_2O^+_{calc.}$	2.74(3)	2.76(2)	2.77(3)
Total	99.21	99.84	99.75
apfu			
^{T}Si	2.99(1)	3.00(2)	3.00(2)
^{T}Al	0.01(0)	0.00(0)	0.00(0)
ΣT	3.00	3.00	3.00
^{M2}Ti	0.00(0)	0.00(0)	0.00(0)
^{M2}Al	0.01(0)	0.01(1)	0.01(1)
^{M2}Sc	0.77(6)	0.76(3)	0.80(6)
$^{M2}Fe^{3+}$	0.14(4)	0.15(3)	0.11(4)
^{M2}Mg	0.08(2)	0.07(2)	0.07(3)
^{M2}Mn	0.00(0)	0.02(0)	0.00(0)
ΣM2	1.00	1.00	1.00
$^{M1}Mn^{2+}$	0.08(2)	0.07(1)	0.07(2)
$^{M1}Mg^{2+}$	0.01(0)	0.00(0)	0.00(0)
^{M1}Ca	0.91(2)	0.93(1)	0.93(4)
ΣM1	1.00	1.00	1.00
^{A}Na	0.01(0)	0.01(0)	0.00(0)
^{A}Ca	0.05(0)	0.05(0)	0.04(0)
ΣA	0.06(0)	0.06(0)	0.05(0)
O	8.03(0)	8.02(0)	8.02(1)
OH	0.97(0)	0.98(0)	0.98(1)

Note: [a] number of spot analyses. H_2O and OH estimates come from charge balancing based on the cascandite stoichiometry.

Table 2. Compositions of the actinolite – scandio-winchite solid-solution members.

	Scandian actinolite			**'Scandio-magnesio-hornblende'**				Scandio-winchite	Refined actinolite
samples	J6	J10	J5	J6	J10	J5	J4	J5	J5
wt.%	n=12[a]	n=15	n=25	n=1	n=2	n=2	n=3	n=2	n=4
SiO_2	57.67(61)	56.68(46)	56.73(46)	56.67	56.37(59)	56.06(14)	56.09(78)	55.86(62)	56.48(16)
TiO_2	0.03(1)	0.03(1)	0.03(2)	0.02	0.03(1)	0.06(2)	0.02(1)	0.03(1)	0.03(2)
Al_2O_3	0.56(13)	0.58(27)	0.54(19)	0.46	0.52(10)	0.67(6)	0.56(4)	1.12(97)	0.42(5)
Sc_2O_3	2.21(33)	2.59(59)	2.29(48)	4.31	3.54(9)	3.92(25)	4.63(28)	4.82(90)	2.11(24)
$Fe_2O_{3\ calc.}$			0.12(42)			0.08(11)		0.02(2)	
MnO	0.32(3)	0.30(4)	0.30(5)	0.38	0.38(5)	0.35(2)	0.32(2)	0.43(12)	0.35(3)
$FeO_{calc.}$	8.00(27)	10.05(51)	7.78(54)	9.35	10.39(29)	8.75(23)	9.03(17)	8.88(17)	7.62(26)
MgO	18.36(40)	16.83(59)	17.95(65)	16.45	15.75(95)	16.51(57)	16.15(59)	15.99(39)	17.76(39)
CaO	9.91(43)	9.92(50)	10.75(61)	9.83	9.85(11)	9.15(64)	9.06(18)	8.09(224)	11.42(30)
Na_2O	0.83(14)	1.01(19)	0.93(16)	1.58	1.40(20)	1.49(10)	1.57(19)	2.20(51)	0.90(17)
K_2O	0.05(1)	0.06(2)	0.05(2)	0.04	b.d.l.	0.06(3)	0.05(2)	0.09(4)	0.03(1)
$H_2O^+_{calc.}$	2.15(2)	2.12(2)	2.13(2)	2.14	2.13(4)	2.10(2)	2.11(3)	2.11(4)	2.12(1)
Total	100.08	100.17	99.61	101.24	100.80	99.21	99.60	99.62	99.23
apfu									
^{T}Si	8.04(3)	7.99(3)	7.98(6)	7.92	7.99(1)	7.96(11)	7.94(1)	7.91(6)	7.98(2)
^{T}Al		0.02(2)	0.03(5)	0.08	0.01(1)	0.06(8)	0.06(1)	0.09(6)	0.02(2)
$^{T}Fe^{3+}$			0.00(1)						
ΣT	8.04(3)	8.01(1)	8.01(2)	8.00	8.00(0)	8.02(2)	8.00(0)	8.00(0)	8.00(0)
^{C}Ti	0.00(0)	0.00(0)	0.00(0)	0.00	0.00(0)	0.01(0)	0.00(0)	0.00(0)	0.00(0)
^{C}Al	0.09(2)	0.08(4)	0.06(3)	0.00	0.08(1)	0.05(7)	0.04(1)	0.09(10)	0.05(1)
^{C}Sc	0.27(4)	0.32(7)	0.28(6)	0.53	0.43(0)	0.49(3)	0.57(4)	0.59(10)	0.26(3)
$^{C}Fe^{3+}$			0.01(4)			0.01(1)		0.00(0)	
$^{C}Fe^{2+}$	0.82(6)	1.06(10)	0.87(8)	1.05	1.17(11)	0.96(5)	0.98(6)	0.92(19)	0.90(3)
^{C}Mg	3.82(8)	3.54(13)	3.76(12)	3.43	3.30(14)	3.49(8)	3.41(8)	3.37(2)	3.74(7)
^{C}Mn	0.00(0)	0.00(0)	0.01(1)	0.00	0.02(2)	0.00(0)	0.00(0)	0.02(3)	0.03(1)
ΣC	5.00(0)	5.00(0)	5.00(0)	5.00	5.00(0)	5.00(0)	5.00(0)	5.00(0)	4.99(1)
$^{B}Mn^{2+}$	0.04(0)	0.04(0)	0.03(1)	0.05	0.02(2)	0.04(0)	0.04(0)	0.03(4)	0.01(1)
$^{B}Fe^{2+}$	0.11(4)	0.12(7)	0.05(5)	0.05	0.05(5)	0.08(1)	0.09(3)	0.13(19)	0.00
^{B}Ca	1.48(7)	1.50(7)	1.62(9)	1.47	1.48(4)	1.39(8)	1.38(3)	1.23(36)	1.73(4)
^{B}Na	0.22(4)	0.28(5)	0.25(4)	0.43	0.38(6)	0.41(2)	0.43(5)	0.60(13)	0.25(5)
ΣB	1.85(7)	1.93(4)	1.94(5)	1.99	1.94(3)	1.92(11)	1.94(2)	2.00(0)	1.98(1)
^{A}Na			0.01(2)			0.00(0)			0.00(1)
^{A}K	0.01(0)	0.01(0)	0.01(0)	0.01	0.00	0.01(0)	0.01(0)	0.02(1)	0.01(0)
OH	1.99(0)	1.99(0)	1.99(0)	1.99	1.99(0)	1.99(0)	1.99(0)	1.99(0)	1.99(0)

Note: [a] number of spot analyses. H_2O and OH estimates come from charge balancing based on the amphibole stoichiometry.

Table 3. Details on data collection and structure refinement of scandian actinolite.

***Data collection and refinement*:**	
Instrument	XtaLAB Synergy, Dualflex, HyPix diffractometer
X-ray radiation source	Cu*K*α (λ = 1.54184 Å)
Temperature	100.0(2) K
Absorption coefficient	17.445 mm^{-1}
F(000)	831
θ range for data collection	4.89 to 72.228°
θ full	67.684°
Index ranges	$-11 \leq h \leq 12$, $-22 \leq k \leq 22$, $-6 \leq l \leq 6$
Reflections collected	7176
Independent reflections	935 [R_{merge} = 0.0502]
Reflections with $I_o > 2\sigma I$	787
Completeness to θ = 71.98°	99.9%
Refinement method	Full-matrix least-squares on F^2
Parameters / restraints	103 / 1
Goodness-of-fit on F^2	1.032
Final *R* indices	R_1 = 0. 0587 [$I_o > 2\sigma(I)$]
	wR_2 = 0.1570 [all data]
Largest diff. peak and hole	0.84 and -0.86 *e*/Å^3, rms = 0.203
***Crystal data*:**	
Refined formula	$Al_{0.06}Ca_{1.57}Fe_{0.56}H_2KMg_{3.83}Na_{0.42}O_{24}Sc_{0.62}Si_{7.94}$
Crystal size	0.02 × 0.008 × 0.017 μm
Crystal system	monoclinic
Space group	*C*2/*m*
Unit-cell dimensions	*a* = 9.8517(3) Å *b* = 18.0881(6) Å *c* = 5.28502(18) Å α = 90º β = 104.809(4)º γ = 90º
Unit-cell volume	*V* = 910.49(6) Å^3
Z	2
Calculated density	3.048 g·cm^{-3}

*$R_{int} = \Sigma|Fo^2 - Fo^2_{(mean)}|/\Sigma[Fo^2]$. GooF = $S = \{\Sigma[w(Fo^2 - Fc^2)^2]/(n-p+r)\}^{1/2}$.
$R_1 = \Sigma||Fo| - |Fc||/\Sigma|Fo|$. $wR_2 = \{\Sigma[w(Fo^2 - Fc^2)^2]/\Sigma[w(Fo^2)^2]\}^{1/2}$; $w = 1/[\sigma^2(Fo^2) + (aP)^2 + bP]$, where *a* is 0.1287, *b* is 0.0000 and *P* is $[2Fc^2 + Fo^2)]/3$.

Table 4. Assigned site-populations, site-scattering and mean bond-lengths for scandian actinolite.

Site	Population	**Site scattering (e^-)**		**Mean bond-length (Å)**	
		ref.	calc. [a]	ref.	calc. [a]
T(1)	Si_4	56.00	56.00	1.622	1.620
T(2)	$Si_{3.98}Al_{0.02}$	55.93	55.98	1.636	1.622
^{C}M(1)	$Mg_{1.594}Fe^{2+}_{0.386}Mn_{0.020}$	29.18(28)	29.66	2.080	2.093
^{C}M(2)	$Sc_{0.249}Mg_{1.476}Fe^{2+}_{0.255}Mn_{0.020}$	29.56(29)	30.07	2.082	2.092
^{C}M(3)	$Mg_{0.739}Fe^{2+}_{0.201}Al_{0.060}$	14.56(18)	14.87	2.072	2.081
ΣC		73.30(75)	74.61		
^{B}M(4)	$Na_{0.29}Ca_{1.71}$	36.18(29)	37.39	2.511	2.498
A	$\square_{0.995}K_{0.005}$	0.19	0.10	2.963	2.95
W	$(OH)_2$			0.98	

Note: [a] data derived from the optimized formula.

Table 5. Bond-valence analysis for scandian actinolite (v.u.)[a].

	A	M(4)	M(1)	M(2)	M(3)	T(1)	T(2)	H3	Σ
O1			$0.357^{x2\downarrow}$	$0.324^{x2\downarrow}$	$0.347^{4\downarrow}$	1.045			2.072
O2		$0.271^{x2\downarrow}$	$0.334^{x2\downarrow}$	$0.359^{x2\downarrow}$			1.013		1.977
O3			$0.373^{x2\downarrow}$		$0.383^{x2\downarrow}$			0.865	1.621
O4		$0.328^{x2\downarrow}$		$0.439^{x2\downarrow}$			1.072		1.838
O5	$0.000^{x4\downarrow}$	$0.113^{x2\downarrow}$				0.975	0.928		2.016
O6	$0.000^{x4\downarrow}$	$0.209^{x2\downarrow}$				0.990	0.881		2.080
O7	$0.002^{x2\downarrow}$					$1.016^{x2\rightarrow}$			2.034
Σ	0.006	$1.839^{x2\rightarrow}$	$2.126^{x2\rightarrow}$	$2.245^{x2\rightarrow}$	2.154	$4.025^{x4\rightarrow}$	$3.895^{x4\rightarrow}$	$0.865^{x2\rightarrow}$	

Note: [a] bond-valence sums were calculated using the equation $S = \exp[(R_0–R)/B]$, where R_0 and B are bond-valence parameters derived by Gagné and Hawthorne (2015), and R is the refined bond length.

632

Pieczka et al._Fig1.tif

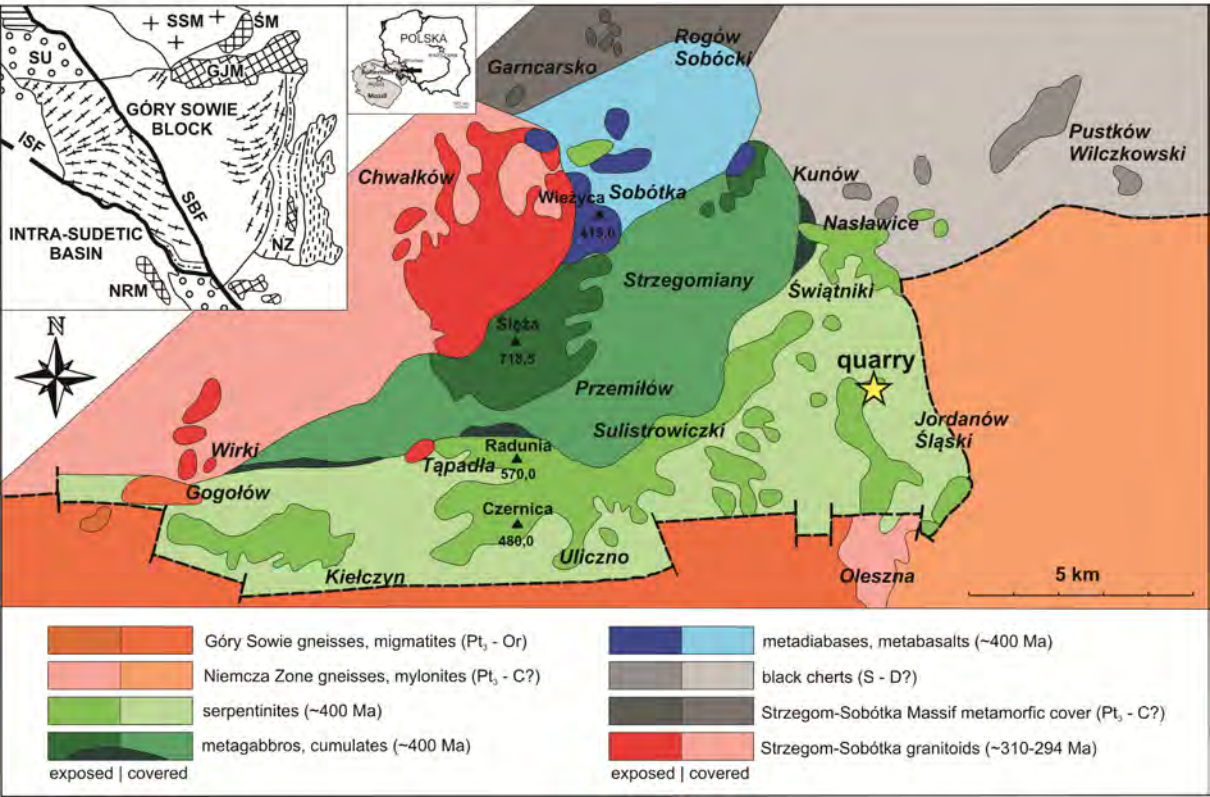

Pieczka et al._Fig2.tif

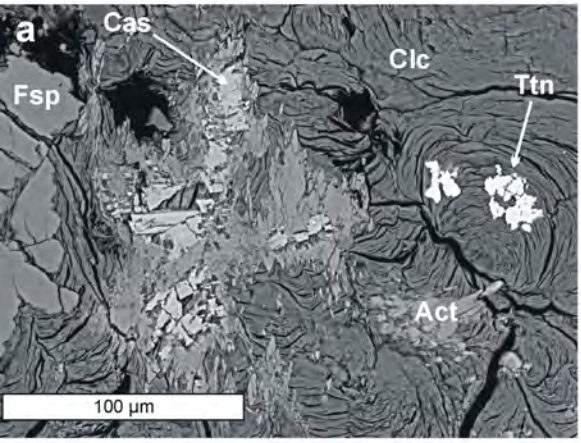

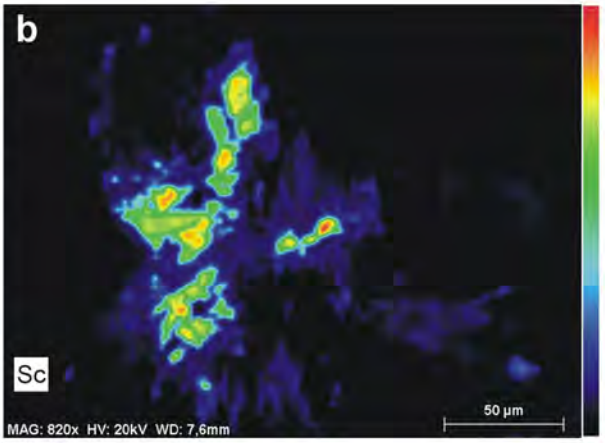

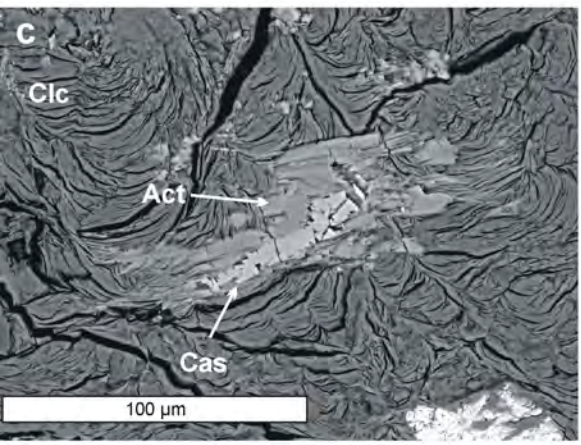

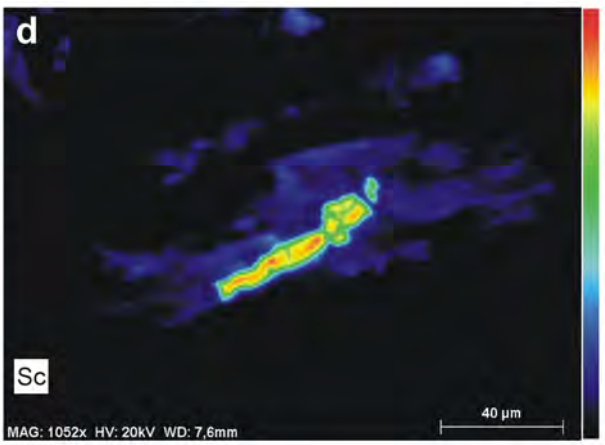

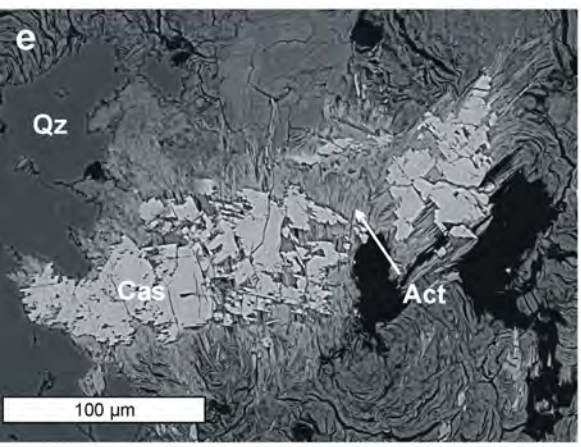

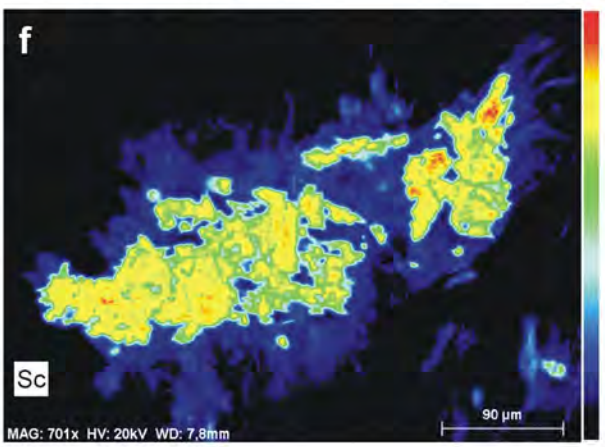

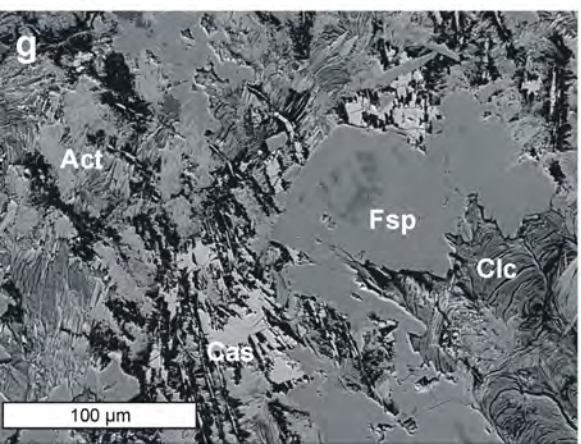

Pieczka et al._Fig3.tif